Journal of Alloys and Compounds 509 (2011) 4357–4362

Contents lists available at ScienceDirect

Journal of Alloys and Compounds

journal homepage: www.elsevier.com/locate/jallcom

First principles calculations on elasticity, electronic structure and bonding properties of antiperovskites $ANTi_3$ (A = Al, In and Tl)

Djellal Cherrad [a,*], L. Selmani [b], D. Maouche [a], M. Maamache [c]

[a] Laboratory for Developing New Materials and their Characterizations, University of Setif, Algeria
[b] University Center of BBA, Algeria
[c] Department of Physics, Faculty of Sciences, University of Setif, Algeria

ARTICLE INFO

Article history:
Received 22 June 2010
Received in revised form 5 January 2011
Accepted 8 January 2011
Available online 15 January 2011

PACS:
74.25.Gz
74.25.Jb
62.20.de

Keywords:
Antiperovskites
Electronic structure
Elastic moduli

ABSTRACT

We use an ab initio pseudopotential plane wave (PP-PW) method within the generalized gradient approximation (GGA) and the local density approximation (LDA) to study the structural, elastic and electronic properties of the unexplored antiperovskite $ANTi_3$ compounds. The elastic constants C_{11}, C_{12}, C_{44} and their pressure dependence are calculated. We derived the bulk, shear and Young's moduli for ideal monocrystalline and for polycrystalline $ANTi_3$ aggregates which we have classified as ductile in nature. Band structures reveal that these compounds are conductors. The covalent ionic bands nature is due to the strong hybridization between Ti 3*d* and N 2*p* states. The Ti 3*d* states play dominant roles near the Fermi levels for all these compounds. The energy difference between spin polarized calculations and the nonspin polarized calculations indicate that $ANTi_3$ compounds exhibit magnetism at their equilibrium lattice constants.

1. Introduction

Intermetallic perovskite nitrides or carbides (formula AXM_3) where X is a main group (III–V) element, A is either carbon or nitrogen, and M is a transition metal [1] display also, a wide range of interesting physical properties and have numerous technological applications, such as giant magnetoresistance [2]. It is called as antiperovskite structure because the transition metals are located at the corners of the octahedron cage in contrast to the ordinary perovskite structure [3]. The intermetallic antiperovskite AXM_3 are related to both classical intermetallics of $AuCu_3$ type and classical oxide perovskites such as $CaTiO_3$ [4]. Among them, $MgCNi_3$ is the first oxygen-free superconductor at 8 K [5], which oriented many experimental and theoretical works towards the investigation of the physical properties of this compound; especially its superconductivity, however, the nature of its superconductivity is still controversial [6]. In order to found uniform behavior in this type of materials, some attention has been paid to the related compounds such as $AlCNi_3$, $CdCNi_3$, $GaCNi_3$, $InCNi_3$ and $ZnCNi_3$. Only $CdCNi_3$ was a superconductor at ~3.4 K [7,8]. The T_c temperature is relatively close to those found recently for the new superconductor $ZnNyNi_3$ at ~3 K [8]. On another hand, the lower T_c of $CdCNi_3$ than that of $MgCNi_3$ was explained by the smaller density of states at the Fermi energy and the enhanced ferromagnetic correlation in $CdCNi_3$ [6].

In order to search a new superconductors antiperovskites, Schaak et al. [4] have synthesized intermetallic perovskite borides and carbides AXM_3 compounds (A = Mg, Ca, Sc, Y, Lu, Zr, Nb; X = B, C; M = Ni, Ru, Rh, Pd, Pt) either by arc melting. The authors have showed that many of these compounds exist over a wide range of stoichiometries, which could critically influence their superconducting properties. Very recently, Cao et al. [8] have synthesized new intermetallic antiperovskite type ternary nitrides $InNCo_3$ from In_2O_3 and Co powders under NH_3 atmosphere at 600 °C with spin glass like behavior. Besides the experimental efforts, many theoretical investigations were also carrying out, especially on the electronic structure and magnetic properties [3,4,6,8,9]. Shim et al. [9] as an example, have performed first principles electronic structure and magnetic calculations using local density approximation LSDA on $GaCMn_3$ and related antiperovskite Mn compounds $ZnNMn_3$, $ZnCMn_3$, and $SnCMn_3$. The authors have confirmed that $SnCMn_3$ compound has a complicated magnetic structure with unstable ferromagnetic FM phase. Mn-based antiperovskite nitrides $ANMn_3$ (A = Cu, Zn, Ga, Ge, etc.) show large negative thermal expansion triggered by AFM or FM transition [8]. It is our ambition to carrying out a ab initio calculation since it was expected

* Corresponding author. Tel.: +213 93 86 36 12.
E-mail address: cherradphisic@yahoo.fr (D. Cherrad).

0925-8388/$ – see front matter © 2011 Elsevier B.V. All rights reserved.
doi:10.1016/j.jallcom.2011.01.042

that the use of new 3d transition metal in antiperovskite nitrides or carbide fascinating the physical properties.

The ternary titanium nitrides $ANTi_3$, where A is from the group III, are isostructural to $MgCNi_3$ and belong to the antiperovskite type compounds. The ideal cubic antiperovskite structure for $ANTi_3$ compounds (#221) contains one formula with the *Wyckoff* positions of the atoms are A 1a (0, 0, 0), N 1b (0.5, 0.5, 0.5) and Ti 3c (0, 0.5, 0.5).

In the present study, lattice parameter, elastic constants, bulk, shear, and Young's moduli and Debye temperature, as well as the electronic structures and magnetic properties of $AlNTi_3$, $InNTi_3$ and $TlNTi_3$ were determined, probably for the first time, in order to fully take advantage of these compounds for eventual technological applications such as superconductivity. Some relationships between the various properties were studied. In addition, we have also compared the properties of $ANTi_3$ with those obtained for $ACTi_3$ compounds.

2. Calculation method

First-principles methods have already used to explore a variety of material properties and shown a good accuracy in the study of many physical and chemical properties for a wide scale of materials [10]. All our investigations were based on density functional theory (DFT). The exchange–correlation potential is treated within the local density approximation (LDA), developed by Ceperley and Alder and parameterized by Perdew and Zinger (CAPZ) [11,12], as well as the generalized gradient approximation (GGA) of Perdew et al. [13] as invoked by the framework package CASTEP Cambridge Serial Total Energy Package [14]. Interactions of electrons with ion cores were represented by the Vanderbilt-type ultrasoft pseudopotential for (N and C), Sn and Mn atoms [15].

The kinetic cut-off energy for the plane wave expansion is taken to be 400 eV, which was large enough to obtain good convergence. In the Brillouin zone integrations, $8 \times 8 \times 8k$ points were determined according to Monkhorst–Pack scheme [16].

Based on the Broyden–Fletcher–Goldfarb–Shenno (BFGS) [17] minimization technique, the system reached the ground state via self-consistent calculation when the total energy is stable to within 5×10^{-6} eV/atom, less than 10^{-2} eV/Å for the maximum ionic Hellmann–Feynman force and maximum stress within 2×10^{-2} eV Å^{-3}.

The elastic coefficients were determined by applying a set of given homogeneous deformations with a finite value and calculating the resulting stress with respect to optimizing the internal atomic degrees of freedoms [18]. The criteria for convergences of optimization on atomic internal freedoms were selected as the difference of total energy within 10^{-6} eV/atom, ionic Hellmann–Feynman force within 2×10^{-3} eV Å^{-1} and maximum ionic displacement within 10^{-4} Å. One strain pattern, with nonzero first and fourth components, in which, two positive and two negative amplitudes were used, gives stresses related to all three independent elastic coefficients for the cubic system.

3. Results and discussion

3.1. Structural properties

First, the equilibrium lattice constants a (Å) for the ideal stoichiometric unexplored antiperovskite $ANTi_3$ with (A = Al, In and Tl) were calculated. The results are listed in Table 1, which are very close to the measured ones [19,20] with small differences due to the reliability of the present first-principles computations. Better theoretical results are obtained with the GGA, since its known that the use of LDA gives slight underestimation (overestimation) of the lattice constants (bulk modulus) [6]. The calculated lattices parameter of $ANTi_3$ compounds increases in the following sequence: a_0 ($ALNTi_3$) < a_0 ($InNTi_3$) < a_0 ($TlNTi_3$). This can be understood from the fact that the atomic radius of Tl (1.7 Å) is larger than that of In (0.8 Å) and Al (0.535 Å) [21].

The bulk modulus B at zero pressure and its pressure derivative B' are calculated by fitting pressure volume data to a third order Birch–Murnaghan equation of state (EOS) [22], employing a dense sampling technology in the low pressure region. Hence our results for B are good and accurate (Fig. 1). Since we are note aware with any previous theoretical result on $ANTi_3$ compounds, our values of B are compared to those calculated for $ACTi_3$ by Medkour et al. [23] which were somewhat close to our one. In addition, our results were compared to those obtained for the first antiperovskite superconductor $MgCNi_3$: the measured value of the bulk modulus of $MgCNi_3$ is ~157 GPa [24], while the calculated ones are ~172 and ~207 GPa using GGA and LDA, respectively [6].

Table 1
Calculated a_0 (in Å), B_0 (in GPa) and B' (calculated from Birch–Murnaghan EOS fitting) compared to experiment data.

	Present work		Experiments
	GGA	LDA	
$AlNTi_3$			
a_0	4.1123	4.051	4.112 [19]
B_0	162.88 ± 0.13	183.41 ± 0.21	
B'	4.054 ± 0.01	4.027 ± 0.02	
$InNTi_3$			
a_0	4.195	4.116	4.190 [20]
B_0	152.961 ± 0.14	183.41 ± 0.21	
B'	4.220 ± 0.01	4.027 ± 0.02	
$TlNTi_3$			
a_0	4.204	4.124	4.191 [20]
B_0	152.557 ± 0.5	183.40 ± 0.19	
B'	4.335 ± 0.05	4.029 ± 0.02	

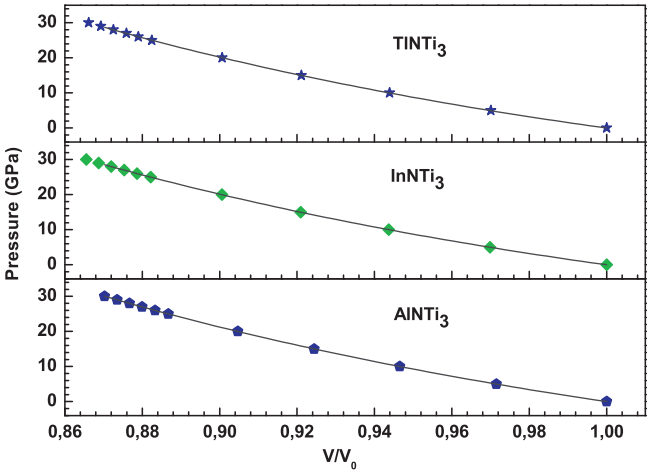

Fig. 1. Calculated pressure–volume relation for $ANTi_3$ compounds. V_0 is the equilibrium volume. The solid lines are given by the Birch–Murnaghan equation of state; parameters are listed in Table 1.

3.2. Elastic properties

The elastic constants of $ANTi_3$ compounds are listed in Table 2. The errors quoted for C_{ij} values are associated with the deviation of the stress strain relationship from linearity [25]. The three independent elastic constants in a cubic symmetry (C_{11}, C_{12}, and C_{44}) were estimated by calculating the stress tensors on applying strains to an equilibrium structure with applied pressure up to 30 GPa. Kumar et al. [24] has reported in experimental work that no phase transition for $MgCNi_3$ was observed for applied pressure up to 32 GPa. All C_{ij} constants for $ANTi_3$ compounds are positive and satisfy the criteria [26] for mechanically stable crystals else the ones obtained from GGA calculations for $InNTi_3$. This result can be explained by the underestimation associated with the use of GGA but experimental confirmation is necessary:

$$C_{44} - P > 0 \quad (1)$$

$$\frac{(C_{11} - C_{12})}{2} - P > 0 \quad (2)$$

$$\frac{(C_{11} + 2C_{12} + P)}{3} > 0 \quad (3)$$

Table 2
Calculated zero pressure C_{ij}, B as $B=(C_{11}+2C_{12})/3$, A, G, E, λ, μ and σ for ideal monocrystalline and for polycrystalline $ANTi_3$ aggregates.

	C_{11}		C_{12}		C_{44}		B		A	
	GGA	LDA	GGA	LDA	GGA	LDA	GGA	LDA	GGA	LDA
$AlNTi_3$										
*	199.42 ± 3.4	239.94 ± 2.3	146.86 ± 1.1	156.60 ± 0.4	50.72 ± 0.4	57.91 ± 0.4	164.38 ± 1.4	184.38 ± 0.8	1.9299	1.389
**	–	–	–	–	–	–	–	–	–	–
$InNTi_3$										
*	137.69 ± 2.1	189.85 ± 1.8	161.35 ± 0.5	171.05 ± 0.9	38.54 ± 0.04	49.68 ± 0.8	–	–	–	–
**	–	–	–	–	–	–	153.47 ± 0.7	177.32 ± 0.8	−3.2578	5.2851
$TlNTi_3$										
*	198.00 ± 1.9	256.36 ± 1.2	128.31 ± 1.1	138.44 ± 0.4	52.62 ± 0.3	63.76 ± 0.2	–	–	–	–
**	–	–	–	–	–	–	−151.54 ± 0.9	177.75 ± 0.4	1.5101	1.0814

	G		E		μ		λ		σ	
	GGA	LDA	GGA	LDA	GGA	LDA	GGA	LDA	GGA	LDA
$AlNTi_3$										
*	–	–	74.851	116.240	50.720	57.916	97.987	124.108	0.4241	0.3949
**	38.956	50.756	108.311	139.472	38.956	50.756	138.409	150.542	0.3901	0.3739
InNTi3										
*	–	–	−36.424	27.712	38.543	49.685	60.609	90.486	0.5396	0.4740
**	−18.21	25.93	−56.880	74.191	−18.210	25.936	165.603	160.025	0.5617	0.4302
TlNTi3										
*	–	–	97.097	159.263	52.621	63.760	92.764	128.841	0.3932	0.3507
**	44.606	61.794	121.862	166.131	44.6063	1.7945	121.802	136.550	0.3659	0.3442

* Single crystal.
** Polycrystalline aggregates.

Cracks in crystals are directly related to the anisotropy of thermal and elastic properties [27]. We have also calculated the anisotropy factor A (Table 2.) of our compounds using the following expression for cubic symmetry:

$$A = \frac{2C_{44}}{C_{11} - C_{12}} \tag{4}$$

We present the variation of the elastic constants (C_{11}, C_{12} and C_{44}) and the bulk modulus B of $ANTi_3$ compounds with respect to the variation of pressure In Fig. 2. We clearly observe a linear dependence in all curves of both compounds in the considered range of pressure. From Tables 1 and 2, we can see that the calculated values of the bulk moduli B from the elastic constants ($B=(C_{11}+2C_{12})/3$) have nearly the same values as the ones obtained from the (EOS) fitting. This might be an estimate of the reliability and accuracy of our calculated elastic constants for $ANTi_3$. Additionally, we note that our obtained values for B using LDA are somewhat unrealistic; a fact gives the GGA a better accuracy than LDA.

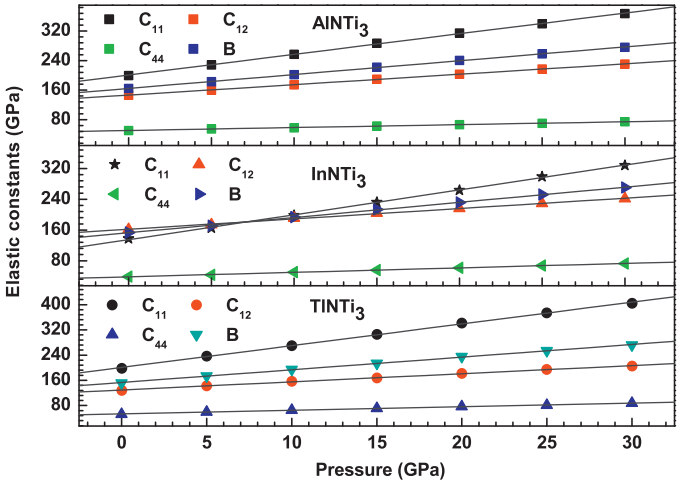

Fig. 2. Pressure–elastic constants dependence of $ANTi_3$ compounds. The solid lines are least-square linear fits of the data points.

The above elastic parameters are obtained from first-principles calculations of $ANTi_3$ monocrystals, a problem arises when single crystal samples cannot be obtained, for now, it is not possible to measure the individual elastic constants C_{ij}. Instead, the isotropic bulk modulus B and shear modulus G are determined. For this purpose we have utilized the Voigt–Reuss–Hill approximations, this approach says that the actual effective modulus for polycrystals could be approximated by the arithmetic mean of the two well-known bounds for monocrystals according to Voigt and Reuss, while Hill takes the average of both [22] given by:

$$G = \frac{G_V + G_R}{2} = \frac{1}{2}\left[\frac{C_{11} - C_{12} + 3C_{44}}{5} + \frac{5C_{44}C_{11} - 5C_{44}C_{12}}{4C_{44} + 3C_{11} - 3C_{12}}\right] \tag{5}$$

The Young's modulus E which expresses the resistance of material to unidirectional strain, Poisson's ratio σ and the Lame coefficients λ and μ are frequently measured for polycrystalline materials characterizing their hardness [22,27]. These quantities are given by the following equations [28]:

$$E = \frac{9BG}{3B + G} \tag{6}$$

$$\lambda = \frac{E\sigma}{1 - \sigma - 2\sigma^2} \tag{7}$$

$$\mu = \frac{E}{2 + 2\sigma} \tag{8}$$

$$\sigma = \frac{3B - E}{6B} \tag{9}$$

The calculated and the deduced values of B, G, E, λ, μ and σ for single crystal and polycrystalline aggregates of $ANTi_3$ compounds are listed in Table 2.

In Table 3, we listed the pressure derivatives $\partial C_{ij}/\partial P$ and $\partial B/\partial P$ of $ANTi_3$ compounds.

Pugh's [29] empirical relationship says that the simple B/G ratio can classify materials as ductile or brittle according to a critical value separates both behaviors at around 1.75, so if the B/G ratio is greater than 1.75 the material behaves as ductile, otherwise the material behaves as brittle. In a similar fashion, it has been suggested that the ratio of bulk and C_{44} represents a measure for ductile

Table 3
Calculated pressure derivatives of C_{ij} and B for $ANTi_3$ compounds.

	$\partial C_{11}/\partial P$		$\partial C_{12}/\partial P$		$\partial C_{44}/\partial P$		$\partial B/\partial P$	
	GGA	LDA	GGA	LDA	GGA	LDA	GGA	LDA
$AlNTi_3$	5.597	5.543	2.820	2.732	0.787	0.772	3.746	3.669
$InNTi_3$	6.467	6.931	2.689	2.560	1.156	1.111	3.948	4.017
$TlNTi_3$	6.902	6.924	2.571	2.582	1.139	1.095	4.014	4.030

Table 4
Calculated density ρ in (g/cm^3), υ_l, υ_t and υ_m, respectively (in m/s), calculated from polycrystalline elastic moduli, and θ_D in ($^\circ K$) for $ANTi_3$ compounds.

Compounds	ρ		υ_l		υ_t		υ_m		θ_D	
	GGA	LDA	GGA	LDA	GGA	LDA	GGA	LDA	GGA	LDA
$AlNTi_3$	4.410	4.611	6849	7393	2906	3317	3285	3742	407	470
$InNTi_3$	6.129	6.486	5867	5879	2697	2057	3039	2338	369	283
$TlNTi_3$	8.091	8.570	5106	5509	2697	2685	3015	3016	365	372

behavior. Diamond and Al, for example, have a bulk modulus to C_{44} ratio of 0.8 and 2.6, respectively [30]. We have found that the B/G ratios are 3.63, 6.83 and 2.87 and B/C_{44} ratios are 3.81, 3.57 and 2.78 for $AlNTi_3$, $InNTi_3$, $TlNTi_3$, respectively, classifying these materials as ductile.

The Debye temperature is a fundamental parameter in solids, closely related to many physical properties such as elastic constants, specific heat and melting temperature [31]. Using the average sound velocity, we have deduced the Debye temperature θ_D of $ANTi_3$ compounds according to the following equation [31]:

$$\theta_D = \frac{h}{k_B}\left[\frac{3q}{4\pi}\cdot\frac{N\rho}{M}\right]^{1/3}\cdot \upsilon_m \tag{10}$$

where h is Plank's constant, k_B is Boltzmann's constant, N is Avogadro's number, ρ is the density, M is the molecular weight of the solid and q is the number of atoms in the molecule. The average sound velocity in the polycrystalline material is given by [31]:

$$\upsilon_m = \left[\frac{1}{3}\left(\frac{2}{\upsilon_t{}^3}+\frac{1}{\upsilon_l{}^3}\right)\right]^{1/3} \tag{11}$$

where υ_l and υ_t designate the longitudinal and transverse sound velocity obtained from Navier's equation [31]:

$$\upsilon_t = \left(\frac{3B+4G}{3\rho}\right)^{1/2} \quad \text{and} \quad \upsilon_l = \left(\frac{G}{\rho}\right)^{1/2} \tag{12}$$

The above-calculated parameters of our compounds are given in Table 4. Unfortunately, there are no data available in the literature on these properties for these compounds, to our knowledge but future experimental investigation will test our calculated results.

3.3. Electronic and bonding properties

For $ANTi_3$ compounds at their equilibrium lattice constants, the LDA and GGA calculations give almost identical electronic band structures around the Fermi energy level E_F. We therefore discuss only the GGA electronic and bonding results in this section.

The band structure, total (TDOS), atomic site projected densities of states (PDOS) and bonding charge density of these compounds, which have been calculated for the equilibrium geometry of $ANTi_3$ compounds, are shown in Figs. 3 and 4, respectively.

Energy band structure of $ANTi_3$ compounds along the high symmetry lines in the first Brillouin zone is shown in Fig. 3. The non-existence of a gap at Fermi level confirms the metallic character and indicates the respective presence of conducting features.

The calculated total (TDOS) and atomic site projected densities of states (PDOS) of these compounds are shown in Fig. 4.

The origin of the band structure spectra is due to A s, A p, N p, with slight contributions from Ti s, Ti p, and Ti d states in the energy range of −7.6 to 3.2 eV. From 3.2 eV to Fermi level, the band structure is originally derived from the A p and Ti d states. The Ti d states remain majority at Fermi level, i.e. the main part of the conductivity is assured by the d electrons of the transition metal Ti, beyond the Fermi level, the band structure spectra is mainly derived from Mn d states hybridized with a few A p, A s and N p electrons. We note that the peaks located near −5 eV and 2 eV correspond to σ bonding and σ* antibonding states, respectively, of Ti 3d and N 2p states. The hybridization of Ti d states with N p states suggests a strong covalent bonding contribution [32] in $ANTi_3$ compounds.

Since the electrical conductivity is related to the empty states [33], $TlNTi_3$ with a total density of states at the Fermi level $N(EF)_{Total}$ equal to 5.71 is relatively higher than the calculated $TlCTi_3$ one of 4.08 states/eV [23]. $TlNTi_3$ should be more like a conductor than $InNTi_3$ and $AlNTi_3$ with $N(EF)_{Total}$ equal to 5.63 and 4.75 states/eV, respectively. We note that, all our compounds are more conductors than $ACTi_3$ compounds calculated by Medkour et al. [23]. The highest value $N(EF)_{Total}$ can be easily explained as follow: First, the Ti d states states at the Fermi level E_F and just bellow E_F in $TlNTi_3$ is located higher in energy than the The Ti d states of $InNTi_3$ and $AlNTi_3$, and second, the hybridization Ti 3d-Tl p in $TlNTi_3$ antibonding states (π* antibonding states) is the stronger one.

Total and projected densities of states at Fermi level in antiperovskites compounds are directly proportional to the superconducting parameter [3]. In other side, it has been argued that a strongly defined $N(EF)_{Total}$ could be responsible for the absence of superconductivity, result was found after examining experimental

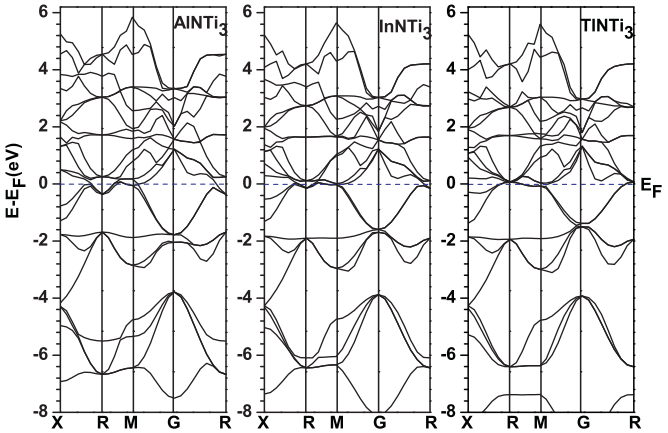

Fig. 3. The calculated band structure of $ANTi_3$ compounds. The vertical dashed line designates the Fermi level E_F.

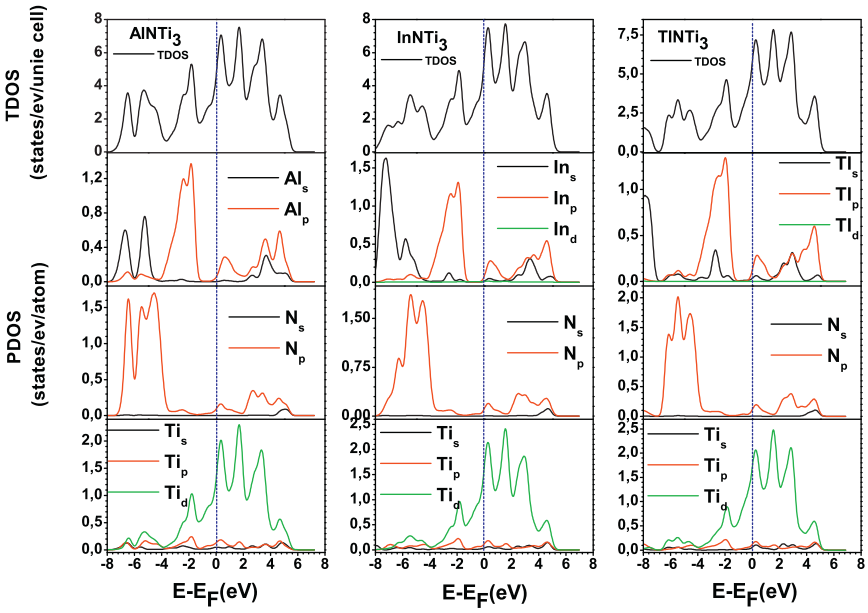

Fig. 4. The calculated total and partial density of states of $ANTi_3$ compounds.

Table 5
Calculated total and partial (projected) DOS at E_F for $ANTi_3$ compounds.

Compounds	$N(EF)_{Total}$		$N(EF)_A$		$N(EF)_N$		$N(EF)_{Ti}$		$N(EF)_{Ti}$	
	GGA	LDA	GGA	LDA	GGA	LDA	GGA	LDA	GGA	LDA
$AlNTi_3$	4.57	4.12	0.053	0.047	0.091	0.082	1.46	1.32	1.29	1.15
$InNTi_3$	5.63	5.09	0.10	0.96	0.11	0.10	1.81	1.63	1.65	1.49
$TlNTi_3$	5.71	5.03	0.16	0.14	0.11	0.10	1.88	1.66	1.69	1.49

data of $ZnCNi_3$ which was smaller than $MgCNi_3$ [7]. The calculated $N(EF)_{Total}$, $N(EF)_A$, $N(EF)_N$, $N(EF)_{Ti}$ and also $N(EF)_{Ti\ d}$ projected densities at E_F for these compounds are given in Table 5. It can be noted that the $N(EF)_{Ti\ d}$ was also estimated since it was found that the contribution of Ni 3*d* states to the superconductivity in $MgCNi_3$ is most important [3]. We have found that in all cases of $AlNTi_3$ compounds, the DOS at the E_F is dominated by Ti 3*d* states with about 29% proportion of the total DOS which is greatly smaller than the calculated one by Wu et al. [6] ~82% in $MgCNi_3$ and $CdCNi_3$. The total densities of states of our compounds exhibit three remarkable and sharp Van Hove singularity peaks just above the E_F were found at 360, 270 and 260 meV for $AlNTi_3$, $InNTi_3$ and $TlNTi_3$, respectively, as shown in Fig. 4. These downward shifts of Van Hove singularity at probably lead to the decrease of the $N(EF)_{Total}$ in $ANTi_3$ compounds. In order to examine the possibility of magnetism in the $ANTi_3$ compounds, we have also performed spin polarized calculations and found that the total energies by the spin polarized calculations are not equal to the values by the non spin polarized calculations. Our results indicate that $ANTi_3$ exhibit magnetism at their equilibrium lattice constants by both the LDA and GGA calculations. The GGA energy difference between none polarized or the spin glass state and spin polarized were 2.1×10^{-4}, −0.051 and −0.0095 eV for $AlNTi_3$, $InNTi_3$ and $TlNTi_3$, respectively. These results may lead to lower T_c or no superconducting behavior in our compounds.

Besides whether, the estimation of the most stable magnetic states can be done using the energy difference $\Delta E = E$(none spin polarized or spin glass state) − E(ferromagnetism state). $\Delta E > 0$ corresponds to the fact that the ferromagnetic phase is more stabilized than anti ferromagnetic phase, and vice versa. Hence fore, the most stable magnetic state of $AlNTi_3$ is of ferromagnetism while are of anti-ferromagnetism in both $InNTi_3$ and $TlNTi_3$.

Fig. 5, shows the charge density contour in the (1 1 0) plane for cubic antiperovskite $InNTi_3$ which was choosing as a prototype since the details of the chemical bonding are rather similar. It can be seen that there is interaction of charges between N and Ti due to N 2*p* and Ti 3*d* hybridization, thus showing that there is covalent bonding between nitrogen and titanium. The near spherical charge distribution around the indium site is comparatively negligible and as a result, the indium atom is fairly isolated which could indicate that the bonding between indium and NTi_3 is mainly ionic.

In Table 6, we have listed the Milliken charge transfer and the overlap population for nearest neighbors in these crystals. The bonding (anti-bonding) states are related to positive (negative) values of bonds population, while the lowest (highest) values imply

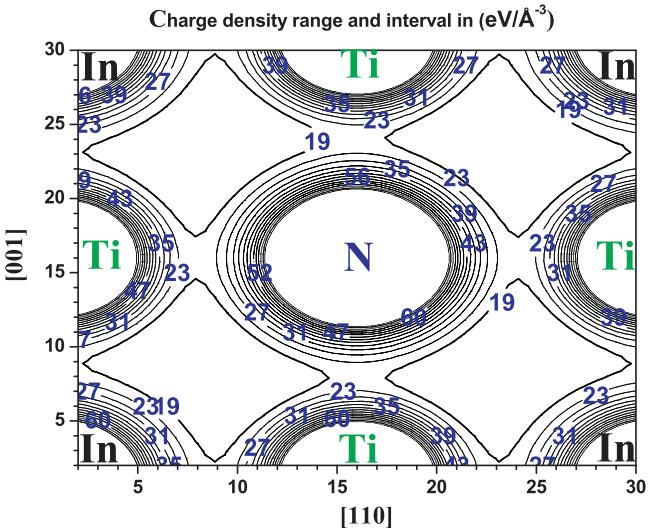

Fig. 5. Valence charge density maps of $InNTi_3$ in the (1 1 0) plane.

Table 6
Calculated zero-pressure Milliken charges, bonds population and bonds lengths for $ANTi_3$ compounds.

Compounds	Species		M. charge	Bond lengths	Bond population
$AlNTi_3$	Al	GGA	−0.17	Al–Ti: 2.9076	0.84
		LDA	−0.14	Al–Ti: 2.8649	0.81
	N	GGA	−0.73	N–Ti: 2.0560	0.53
		LDA	−0.71	N–Ti: 2.0258	0.51
	Ti	GGA	0.30	Ti–Ti: 2.9076	−0.87
		LDA	0.28	Ti–Ti: 2.8649	−0.90
$InNTi_3$	In	GGA	−0.90	In–Ti: 2.9663	−1.76
		LDA	−0.94	In–Ti: 2.9109	−2.08
	N	GGA	−0.73	N–Ti: 2.0975	0.62
		LDA	−0.71	N–Ti: 2.0583	0.59
	Ti	GGA	0.54	Ti–Ti: 2.9663	0.16
		LDA	0.55	Ti–Ti: 2.9109	0.21
$TlNTi_3$	Tl	GGA	−0.83	Tl–Ti: 2.9727	−1.91
		LDA	−0.77	Tl–Ti: 2.9163	−2.48
	N	GGA	−0.76	N–Ti: 2.1020	0.64
		LDA	−0.74	N–Ti: 2.0621	0.61
	Ti	GGA	0.53	Ti–Ti: 2.9727	0.65
		LDA	0.51	Ti–Ti: 2.9163	0.84

that the chemical bond exhibits strong ionic (covalent) bonding [32–36]. In spite of this, In–Ti, Tl–Ti and Ti–Ti of $ANTi_3$ compound listed in Table 6 are in antibonding states. Therefore, it gives rise to π^* and σ^* bands. Bonding states may correlate with the relative high value of the Bulk to shear modulus ratios of these compounds.

$TlNTi_3$ with a valence state of $Tl^{-0.83}N^{-0.76}(Ti^{0.53})_3$ is more covalent than $AlNTi_3$ and $InNTi_3$ with $Al^{-0.17}N^{-0.73}(Ti^{0.30})_3$ and $In^{-0.90}N^{-0.70}(Ti^{0.54})_3$, while the ionicity of these compounds decreases in the following sequence $AlNTi_3 \rightarrow TlNTi_3 \rightarrow InNTi_3$.

Since the decrease of C_{44} is related to the presence of antibonding states during the atomic interaction [37] it can be expected that antibonding states decreases in the sequence $TlNTi_3 \rightarrow AlNTi_3 \rightarrow InNTi_3$. We have found that the population of Ti–Ti in $TlNTi_3$ bonds is higher than Ti–Ti bonds in $InNTi_3$ which probably lead to the highest value of C_{11} in $TlNTi_3$, also, the population of Tl–Ti bonds in $TlNTi_3$ antibonding states is greater than that obtained for In–Ti bonds in $InNTi_3$ lead to the highest value of C_{44} in $TlNTi_3$. Values of the unidirectional elastic modulus C_{11}, C_{44} can be explained as follows: C_{11} is related to the bonding state of Ti–Ti bonds along the principal crystal directions. However C_{44} is related to the antibonding states of A–Ti bonds along the principal crystal directions and results in a weaker resistance to shear deformation or weaker C_{44} of $InNTi_3$. It can be noted that elastic modulus C_{12} is probably related to the bonding states of N–Ti bonds along the principal crystal directions.

4. Conclusions

Employing the (PP-PW) approach based on density functional theory, within the local density approximation and the generalized gradient approximation, we have studied the structural, elastic and electronic properties of $ANTi_3$ compounds. Our main results and conclusions can be summarized as follows:

- The calculated equilibrium lattice constants of these compounds are in reasonable agreement with the available experimental data.
- Bulk moduli provided from fitting the Birch–Murnaghan EOS [22] of the studied compounds, were obtained by employing dense sampling technology in the low-pressure region, hence our results for B are good and accurate.
- The B/G values of $ANTi_3$ compounds show that these materials behave as ductile.
- The band structure calculations show that our compounds are conductors and exhibit magnetism at their equilibrium lattice constants.
- The bonding charge density calculations and the Milliken charge analysis reveal that the chemical bonding in $ANTi_3$ compounds may be covalent–ionic.
- The elastic properties of the studied compounds showed a correlation with the bonding properties.

References

[1] J.B. Goodenough, J.M. Longo, Magnetic and other properties of oxides and related compounds, in: K.-H. Hellwege, O. Madelung (Eds.), Landolt–Bornstein, New Series, Group III, vol. 4a, Springer-Verlag, Berlin, 1970, pp. 126–275.
[2] W.S. Kim, E.O. Chi, J.C. Kim, H.S. Choi, N.H. Hur, Solid State Commun. 119 (2001) 507–512.
[3] J.H. Shim, S.K. Kwon, B.I. Min, Phys. Rev. 64 (R) (1996) 180510.
[4] R.E. Schaak, M. Avdeev, W.L. Lee, G. Lawes, H.W. Zandbergen, J.D. Jorgensen, N.P. Ong, A.P. Ramirez, R.J. Cava, J. Solid State Chem. 177 (2004) 1244–1251.
[5] T. He, Q. Huang, A.P. Ramirez, Y. Wang, K.A. Regan, N. Rogado, M.A. Hayward, M.K. Hass, J.S. Slusky, K. Inumara, H.W. Zandbergen, N.P. Ong, R.J. Cava, Nature 411 (2001) 54.
[6] S.Q. Wu, Z.F. Hou, Z.Z. Zhu, Solid State Sci. 11 (2009) 251–258.
[7] C.M.I. Okoye, Solid State Commun. 136 (2005) 605–610.
[8] W.H. Cao, B. He, C.Z. Liao, L.H. Yang, L.M. Zeng, C. Dong, J. Solid State Chem. 182 (2009) 3353–3357.
[9] J.H. Shim, S.K. Kwon, B.I. Min, Phys. Rev. B 66 (R) (2002) 020406.
[10] S.J. Clark, M.D. Segall, C.J. Pickard, P.J. Hasnip, M.J. Probert, K. Refson, M.C. Payne, Z. Kristallogr. 220 (2005) 567.
[11] D.M. Ceperley, B.J. Alder, Phys. Rev. Lett. 45 (1980) 566–569.
[12] J.P. Perdew, A. Zunger, Phys. Rev. B 23 (1981) 5048–5079.
[13] J.P. Perdew, K. Burke, M. Ernzerhof, Phys. Rev. Lett. 77 (1996) 3865.
[14] M.D. Segall, P.J.D. Lindan, M.J. Probert, C.J. Pickard, P.J. Hasnip, S.J. Clark, M.C. Payne, J. Phys.: Condens. Matter. 14 (2002) 2717.
[15] D. Vanderbilt, Phys. Rev. B 41 (1990) 7892.
[16] J.D. Pack, H.J. Monkhorst, Phys. Rev. B 16 (1977) 1748.
[17] T.H. Fischer, J. Almlof, J. Phys. Chem. 96 (1992) 9768.
[18] V. Milman, M.C. Warren, J. Phys.: Condens. Matter. 13 (2001) 241.
[19] J.C. Schuster, J. Bauer, J. Solid State Chem. 53 (1984) 260–265.
[20] W. Jeitschko, H. Nowotny, F. Benesovsky, Monatsh. Chem. 95 (1964) 436–438.
[21] A.S. Verma, V.K. Jindal, J. Alloys Compd. 485 (2009) 514–518.
[22] J.F. Nye, Propriétés Physiques Des Matériaux, Dunod, 1961.
[23] Y. Medkour, A. Roumili, M. Boudissa, D. Maouche, Solid State Commun. 146 (2009) 919–922.
[24] R.S. Kumar, A.L. Cornelius, Y. Shen, T.G. Kumary, J. Janaki, M.C. Valsakumar, M.F. Nicol, Physica B 363 (2005) 190.
[25] A. Gusev Andrei, M. Zehnder Marcel, W. Suter Ulrich, Phys. Rev. B 56 (1996) 1.
[26] J. Wang, S. Yip, S.R. Phillpot, D. Wolf, Phys. Rev. Lett. 71 (1993) 4182.
[27] D.J. Green, An Introduction to the Mechanical Properties of Ceramics, Cambridge University Press, 1998.
[28] E. Schreiber, O.L. Anderson, N. Soga, Elastic Constants and their Measurement, McGraw-Hill, New York, 1973.
[29] S.F. Pugh, Phil. Mag. 45 (1954) 823.
[30] Denis Music, M. Jochen, Schneider, Appl. Phys. Lett. 89 (2006) 1219144.
[31] O.L. Anderson, J. Phys. Chem. Solids 24 (1963) 909.
[32] N.W. Ashcroft, N.D. Mermin, Solid State Physics, Saunders College, Philadelphia, 1976.
[33] Music Denis, M. Schneider Jochen, Appl. Phys. Lett. 88 (2006) 031914.
[34] M.D. Segall, C.J. Pickard, R. Shah, M.C. Payne, Mol. Phys. 89 (1996) 571.
[35] M.D. Segall, R. Shah, C.J. Pickard, M.C. Payne, Phys. Rev. B 54 (1996) 16317.
[36] Hongsheng Zhao, Aimin Chang, Yunlan Wang, Physica B 404 (2009) 2192–2196.
[37] C. Li, B. Wang, R. Wang, H. Wang, X. Lu, Physica B 403 (2008) 539–543.